Registration of Preoperative Liver Model for Laparoscopic Surgery from Intraoperative 3D Acquisition

Jordan Bano[1,2], Stéphane A. Nicolau[1], Alexandre Hostettler[1], Christophe Doignon[2], Jacques Marescaux[1], and Luc Soler[1,3]

[1] IRCAD, Virtual-Surg, Strasbourg, France
[2] ICube (UMR 7357 CNRS), University of Strasbourg, France
[3] IHU, Institut Hospitalo-Universitaire, Strasbourg, France
jordan.bano@gmail.com

Abstract. Augmented reality improves the information display during intervention by superimposing hidden structures like vessels. This support is particularly appreciated in laparoscopy where operative conditions are difficult. Generally, the displayed model comes from a preoperative image which does not undergo the deformations due to pneumoperitoneum. We propose to register a preoperative liver model on intraoperative data obtained from a rotational C-arm 3D acquisition. Firstly, we gather the two models in the same coordinate frame according to anatomical structures. Secondly, preoperative model shape is deformed with respect to the intraoperative data using a biomechanical model. We evaluate our method on two in vivo datasets and obtain an average error of 4 mm for the whole liver surface and 10 mm for the vessel position estimation.

Keywords: registration, liver, laparoscopy, intraoperative, augmented reality.

1 Introduction

Laparoscopic surgery is a well-know technique that can replace open surgery to improve patient healthcare. However, this kind of surgery is difficult to achieve due to the loss of 3D depth and tactile perceptions during intervention. Augmented reality has been proposed to display structures like liver vessels or tumours that are usually hidden on the video [8,9,13]. This information is usually coming from an image acquired before the intervention and thus without pneumoperitoneum. This gas injection, that creates a working space for surgeons, highly modifies viscera shape and particularly the liver which undergoes deformations over several centimeters [5] and are extremely difficult to simulate [6,7] (cf. Fig. 1). Therefore, it is mandatory to update the preoperative model shape for augmented reality based guidance applications. Obviously, this update can be done only if intraoperative information of the critical structures is available.

C.A. Linte et al. (Eds.): MIAR/AE-CAI 2013, LNCS 8090, pp. 201–210, 2013.

Practically, such information can be provided by organ surface acquisition (using an optical technique) or by intraoperative 3D acquisition (using a rotational C-arm like Zeego SIEMENS). Although rotational C-arms are currently not routinely integrated in surgical rooms, such a set-up begins to be more and more available in hospitals [11,12,14].

In this paper, we propose an approach to update the shape of a preoperative model of the liver using information extracted from an intraoperative 3D volume acquired with a rotational C-arm. To our knowledge, it is the first time that a non-rigid registration of a preoperative 3D model on an intraoperative data acquired after pneumoperitoneum has been evaluated in vivo, in the context of laparoscopic surgery.

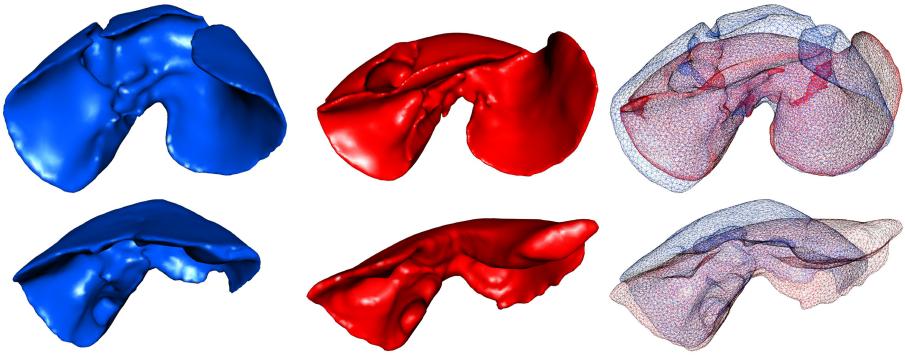

Fig. 1. One can see the porcine liver surface mesh before (resp. after pneumoperitoneum) in the left column (resp. middle column). The two meshes in wireframe (on the right) outline the important deformations that porcine liver undergoes due to pneumoperitoneum: the anterior part shifts down and the left lobe moves toward the left in the abdominal cavity.

Related Work. Vagvolgyi et al. [1] proposed to register a preoperative model of the kidney on an intraoperative surface reconstruction computed from a stereo endoscope. Firstly, a rigid alignment is performed using interactively selected landmarks, refined by an ICP registration. Secondly, a deformation is applied so that the preoperative model fits the reconstructed surface using a mass spring model. The same kind of method is applied for open surgery application, based on a two-step registration (rigid and non-rigid) using surface information from an optical system [3,10,2]. Despite realistic results, no quantitative evaluation was provided on their patient data.

In our context, all these methods cannot provide a good global accuracy. Indeed, the liver undergoes important motion and compression in the antero-posterior direction, but, even if we know the position of the anterior intraoperative part of the liver, the posterior part position remains unknown. One can clearly see in Fig. 1 that an alignment of anterior faces of preoperative and intraoperative liver cannot guarantee a proper registration of the posterior liver part, mainly because of the compression, which makes anterior and posterior

parts closer. Without introperative information of the posterior part, it seems extremely difficult to foresee the liver shape.

Based on this information, we propose a three-step registration method to update the liver preoperative shape from a quick analysis of an intraoperative 3D acquisition. We highlight that our method does not rely on the intraoperative image quality, which is usually poor due to low dose parameters and inserted instruments or trocars, and quite common with rotational C-arm. Moreover, the acquired volume must not necessarily contain the whole liver but a reasonable part of its anterior surface, the spine and the portal vein entry for the initial alignment step of our method.

Firstly, we describe our three-step registration and the data that we have to extract from intraoperative images (cf. Sec. 2). Secondly, we will present the evaluation of our method on two porcine data sets showing that such an approach can provide an updated 3D model with an accuracy within 3 mm for liver surface and 10 mm for vessels (cf. Sec. 3).

2 Method

Our registration is composed of three intraoperative steps. Firstly, a global rigid registration is proposed to align the posterior part of the liver shape of both models in the same space using spine and portal vein entry positions. Then, we compute a matching between the two anterior surfaces using an interactive tool based on geodesic distance analysis. Finally, this matching is used to update the preoperative model shape from a biomechanical simulation engine.

2.1 Pre-processing of Data Input

The liver and critical structures (vessels and tumours) are segmented on the preoperative acquisition by experts using semi-automatic tools and corresponding surface meshes are computed (M_P being the preoperative liver model in this paper). A volume mesh Vm_P is also computed for the liver with the CGAL library (http://www.cgal.org), which is required for the biomechanical deformation step.

We assume that the liver posterior part does not undergo deformations due to pneumoperitoneum (cf. Fig. 2). This assumption seems quite reasonable since analysis of two pairs of 3D acquisitions of pigs (before and after pneumoperitoneum) shows that shape deformation in this part is small. Indeed, ICP rigid registration of the posterior part leads to surface registration errors of 1 mm on average. The spine undergoes a little deformation during gas injection and can thus be used as a landmark to estimate the liver posterior part position. Segmentation of the spine is done automatically with a threshold of the intraoperative medical image and by keeping the largest connected component. However, the liver can slide a little along the spine (cranio-caudal direction) although it is attached to vena cava and aorta. Relying on spine registration only is thus not sufficient and a further translation is necessary. We decided to use the main

portal vein bifurcation, visible in both preoperative and intraoperative images to compute this translation.

For the non-rigid registration step, the anterior surface of the liver in the intraoperative image M_I is necessary and segmented (cf. Fig. 3): firstly, we threshold the air (around -1000 HU) and we compute the two main connected components which are the air around the patient and the air in the abdominal cavity. Then, we keep the part of tissue (between 100 HU and 210 HU) which is connected to the air in the abdominal cavity only. The other viscera such as stomach and bowels are also extracted with this method. Thus, a manual step is required to delineate the liver area only on the surface model. The mesh curvature close to liver boundaries, allows an easy visual identification (and could be automatized in the future).

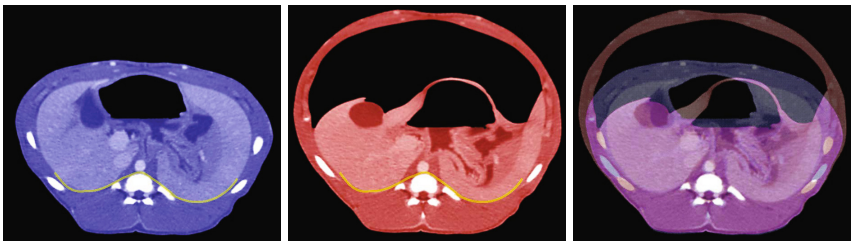

Fig. 2. One can see that the posterior part of the liver is not much deformed after pneumoperitoneum. On the left: the image before pneumoperitoneum, on the right: the image after pneumoperitoneum. The left image was rigidly registered according to the spine position and the portal vein entry point. On both images, we highlight in yellow the liver posterior part. One can see on the right image that the liver shape remains almost identical after pneumoperitoneum.

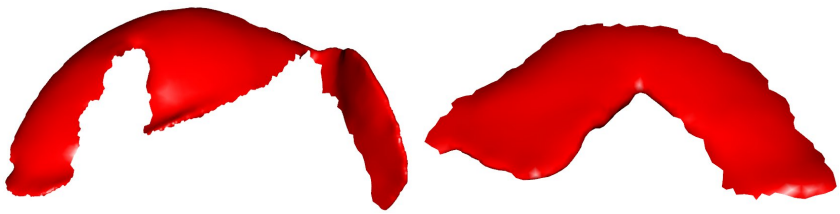

Fig. 3. On both figures, one can see the anterior part of the liver after pneumoperitoneum extracted with our method.

2.2 Rigid Registration Using Anatomical Landmarks

In this step, we rigidly register the preoperative and the intraoperative model using the spine position and the portal vein entry point. A first ICP rigid registration is performed between both meshes of the spine. The translation of this rigid registration is then refined using a manual identification of the portal vein entry point in both 3D images, easily identified despite the low quality of the C-arm acquisition (cf. Fig. 4).

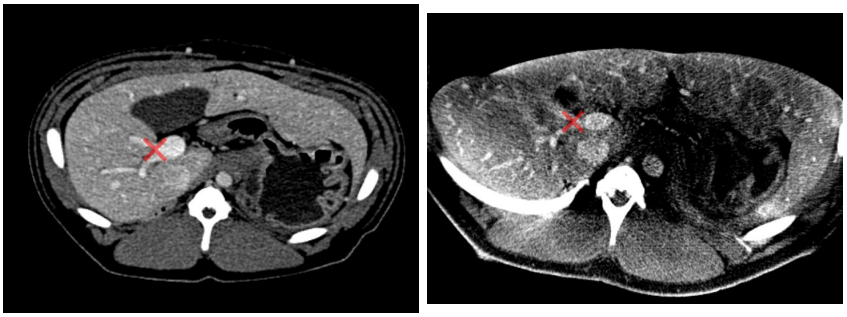

Fig. 4. One can see the preoperative CT (on the left) and the C-arm 3D acquisition (on the right). The bifurcation of the portal vein we use to refine the translation is highlighted with a red cross.

2.3 Vertex Matching between M_P and M_I

In the previous step, the preoperative model M_P was rigidly registered on M_I so that when superimposed, their posterior part is on top of each other. The next step is the computation of the vertex matching between anterior parts of M_P and M_I. This matching step is performed using geodesic distances on meshes between vertices and relevant anatomical landmarks.

These landmarks are manually identified and matched on both meshes. We call a geodesic distance map GDM_L the set of geodesic distances between each mesh vertex and a landmark L. The geodesic distance is the length of the shortest path along the mesh between two vertices and is computed with the *geodesic* library (http://code.google.com/p/geodesic/). We assume that the geodesic distance of a vertex V_P to a landmark on M_P is approximately the same as the distance between the corresponding vertex V_I and the matched landmark on M_I (cf. Fig. 5). Practically, three GDM associated to three landmarks are sufficient to compute all vertex matches.

For each vertex V_I, we compute its anatomical corresponding V_C on M_P which minimizes the following criteria:

$$V_C = \underset{V_k \in M_P}{\arg\min} \sum_{L_I^j, L_P^j \in LandmarkSet} ||(GDM_{L_I^j}(V_I) - GDM_{L_P^j}(V_k))|| \bullet \delta,$$

$$\text{where } \delta \text{ is a normalized weight: } \delta = \frac{[GDM_{L_I^j}(V_I)]^{-1}}{\sum_{i \in [0;NbLandmark]} [GDM_{L_I^i}(V_P)]^{-1}} \quad (1)$$

(which increases when V_I is close to the landmark L_I^j)

2.4 Biomechanical Deformation

The resulting matches provide a displacement field of the liver anterior surface. A biomechanical model is then used to interpolate this field on the liver inner

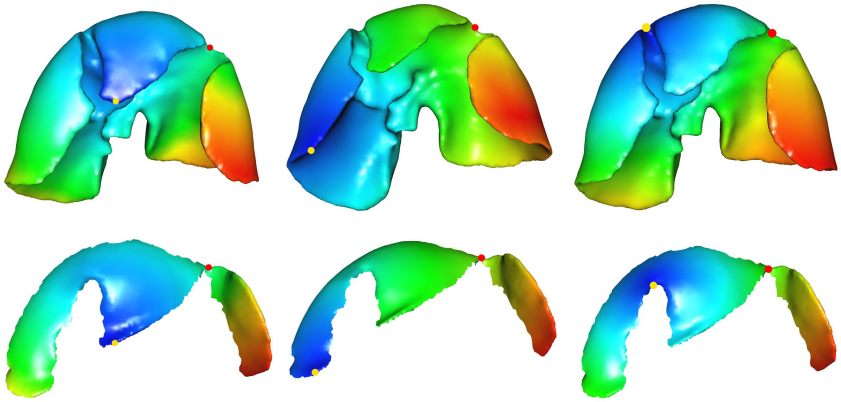

Fig. 5. One can see the preoperative liver mesh M_P (top row) and the liver anterior part after pneumoperitoneum M_I (bottom row) obtained from the method in Sec. 2.1. Colours on each mesh illustrate the geodesic distance of each vertex to a landmark (the yellow point). Blue vertices are close to the landmark and red ones are far. One can see that anatomically matched vertices have approximately the same colour (the red point is an example).

part. The volume mesh of the preoperative mesh is associated with a finite element model for soft tissue deformation. M_P and this volume mesh are mapped together: each vertex of M_P is associated with a tetrahedron of Vm_P. Thus, if a displacement is applied on a vertex of M_P, a corresponding displacement is propagated to the associated tetrahedron of Vm_P using the transpose of the Jacobian of the mapping. In a same way, the vessel mesh is mapped with Vm_P: when Vm_P is deformed, the vessels are also deformed. We assume that the liver posterior part is not deformed during pneumoperitoneum, thus, the posterior vertices of M_P are fixed (cf. Fig. 6). The deformation of M_P is finally performed by adding springs between the matched points with a stiffness selected empirically so that M_P overlaps M_I (cf. Fig. 6).

The biomechanical parameters used for the finite element model are Young's modulus and Poisson ratio. These parameters represent the elasticity and compressibility properties of the liver. We choose realistic values found in literature for Young's modulus (15 kPa found in [4]). The Poisson ratio is equal to 0.35 to allow slight volume compression or dilation. Indeed, it happens that the volume of the liver slightly changes during pneumoperitoneum.

3 Evaluations on Porcine Data

Our evaluation is performed on data from two pigs: a pair of 3D volume data sets has been acquired with contrast agent before and after pneumoperitoneum for both pigs. For the first pair, the pig stayed on the same CT table, so that the rigid registration based on spine was not necessary (only translation had to be estimated). For the second pair, the pig was moved from a CT to a Zeego

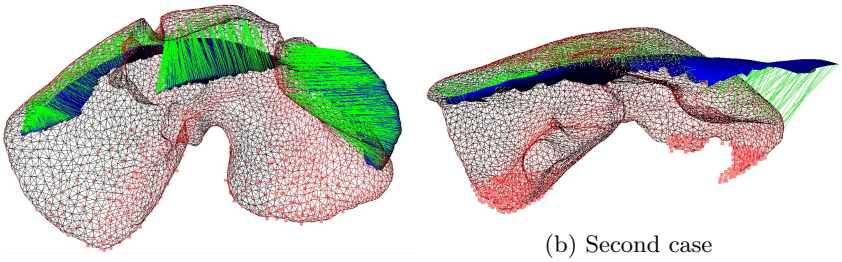

(a) First case (b) Second case

Fig. 6. One can see the two meshes before our biomechanical deformation using SOFA for the two cases. The source mesh is in red and each of its vertices is pulled to match with its matching vertex on the target blue mesh using springs (in green). The fixed points in the posterior part are in pink.

C-arm: preoperative data has been acquired with CT and intraoperatively after pneumoperitoneum on Zeego.

The evaluation requires a ground truth: segmentation of the liver (M_F) and its vessels on the intraoperative acquisition is performed for both cases. We evaluate the registration accuracy of our method on the liver surface and the simulated vessel positions: we compare our registration results with the segmentation of the intraoperative acquisition. The biomechanical simulation is performed using the FEM from the SOFA engine (http://www.sofa-framework.org/).

We highlight that the ground truth liver segmentation was done fully manually on Zeego image due to the acquisition quality: image intensity values in the liver are extremely inhomogeneous due to artefacts.

On average, our method requires about 5 minutes, including all the interactive steps: intraoperative segmentation (1 min), rigid registration (1 min), vertex matching (2 min) and biomechanical deformation (1 min). This duration is a reasonable delay for the surgeon, although it should be reduced to 1 min to be totally accepted in the clinical workflow.

3.1 Evaluation of the Mesh Surface Position

We compare our computed surface mesh M_R with the full intraoperative mesh M_F. We provide a colour scheme for M_R which illustrates the distance between it and M_F. This colour scheme is done by computing the distance between each triangle T_R of M_R and the mesh M_F (i.e. the length of the orthogonal projection of the gravity center G of T_R on the closest triangle of M_F). The contribution of each triangle is weighted according to its area size.

We obtain a mean error within 4 mm for the whole liver in both cases. As a reference we compute the distance between the two input meshes just after the rigid registration and the mean error is 6 mm (for more details cf. Tab.1 and Fig. 7). We also compute the distance before rigid registration for the first case, as the images were acquired within a short delay in the same CT-scan.

The main errors are in the cranial part of the liver. Indeed, the diaphragm is also deformed during pneumoperitoneum which causes deformation of several millimeters, which are difficult to predict since they cannot be easily segmented in the intraoperative images.

Table 1. The distance between each triangle of M_R and the ground truth segmentation is computed and sorted in four groups. Each group contains a quartile of the triangle total number weighted by its area size. The distance is between M_R and M_F: before registration (1), after rigid registration (2) and after non-rigid registration (3).

	First case (mm)			Second case (mm)	
Colour range	(1)	(2)	(3)	(2)	(3)
Blue to Turquoise	0 - 3.4	0 - 1.4	0 - 1.0	0 - 2.9	0 - 1.2
Turquoise to Green	3.4 - 6.2	1.4 - 3.4	1.0 - 2.5	2.9 - 6.3	1.2 - 3.2
Green to Yellow	6.2 - 10.9	3.4 - 8.7	2.5 - 4.2	6.3 - 11.3	3.2 - 6.3
Yellow to Red	10.9 - 54.9	8.7 - 47.1	4.2 - 12.4	11.3 42.2	6.3 - 40.8
Mean (± Std.Dev.)	6.0 (± 7.2)	4.9 (± 6.8)	2.3 (± 2.4)	6.3 (± 7.0)	3.6 (± 4.6)

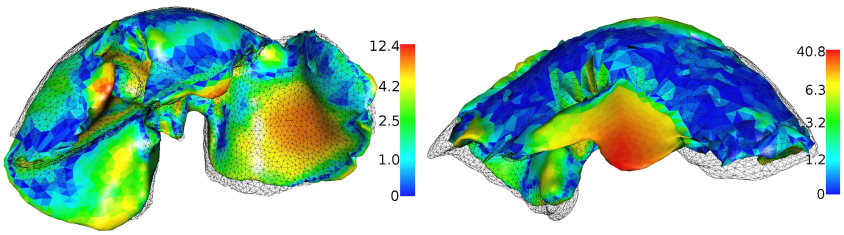

Fig. 7. One can see the results of our method on the liver surface of the examples illustrated in Fig. 1 with the ground truth in black wireframe. Both meshes are coloured according to Tab.1: the left one with the third column and the right one with the fifth column. For the second case on the right, one can see that the results are not very good on the middle part of the liver. In fact, during pneumoperitoneum, the middle liver lobe went to the right under the right lobe. This phenomenon also explains the average surface error of 3.6 mm . Our registration does not manage this kind of displacement for the moment.

3.2 Evaluation of the Vessel System

The evaluation of the vessel registration accuracy is performed on both cases (cf. Fig. 8). We compute the Euclidean distance between some vein bifurcations which have been manually selected. We obtain for the first case (resp. the second case), an average error of 17.5 mm ± 9.0 mm and maximum value 37.4 mm (resp. 14.8 mm ± 10.7 mm and maximum value 38.2 mm) without our registration and 10.3 mm ± 2.7 mm and maximum value 15.8 mm (resp. 10.8 mm ± 8.3 mm and maximum value 28.9 mm) after the non-rigid registration (cf. Fig. 8).

We have observed that the improvement of the non-rigid registration is less important for the second data set due to the lobe sliding phenomenon. Indeed, the non-rigid registration properly compensates for the lobe motion only if lobe

surface is identified and matched on both preoperative and intraoperative images. On the second data set, since one lobe moved and is hidden below another one, we could not perform a proper surface matching. If we ignore this lobe in the error computation (the first error on the right histogram on Fig. 7), the average error decreases to 9 mm ± 2.5 mm. We believe that results should be better on human data since human liver is not composed of independent lobes and has less elastic properties.

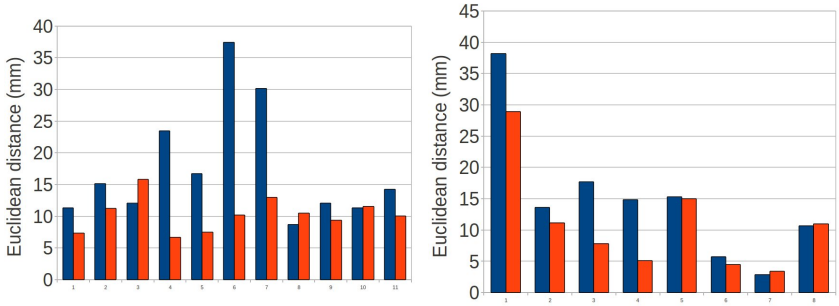

Fig. 8. One can see the Euclidean distance between vessel bifurcations after rigid registration (in blue) and after non-rigid registration (in orange). Each column represents the error of one bifurcation.

4 Conclusion

In this paper, we propose to update a preoperative shape model using intraoperative data from a 3D C-arm acquisition. Firstly, we have shown that a registration based on an anterior surface information only is insufficient to provide good accuracy. To overcome this issue, we have proposed to register the posterior part with the reasonable assumption that it remains rigid. The anterior part deformation is performed with a non-rigid registration corresponding to the anatomical area in the intraoperative image. Results show the feasibility of our approach. We are aware that our method requires manual steps (portal vein entry identification and landmark matching), but it seems reasonable for our clinicians. In fact, the main concern of surgeons is the registration error. Our method still has to be improved since surgeons consider that an acceptable guidance accuracy for deep structures is about 5 mm (for instance to show preoperative resection planning). In case we manage to obtain better intraoperative image quality, our work could be a very good initialization for intensity-based registration which may decrease the registration error of our method. We are currently working with radiologists on acquisition device parameters to improve the image quality.

Finally, we believe that our method can also be used with 3D reconstruction based on the endoscopic video. Indeed, the anterior surface we have segmented for our method is approximately what we can expect from a Structure-from-Motion method. If the endoscope is tracked using an optical tracking system as in [11], the table can be used as a reference to initialize the rigid registration up to a translation (along the table plane), that could be determined by a quick

localization of the portal vein from the endoscopic view. This approach will also be tested in the future and integrated in an augmented reality software to visually assess the registration accuracy of our system.

Acknowledgement. We are gareteful to IHU-Strasbourg for providing the Zeego acquisitions on pigs.

References

1. Vagvolgyi, B., et al.: Video to ct registration for image overlay on solid organs. In: Proc. Augmented Reality in Medical Imaging and Augmented Reality in Computer-Aided Surgery (AMIARCS), pp. 78–86 (2008)
2. Rucker, D.C., et al.: Nonrigid liver registration for image-guided surgery using partial surface data: A novel iterative approach. In: SPIE Medical Imaging, p. 86710B. International Society for Optics and Photonics (2013)
3. Cash, D.M., et al.: Compensating for intraoperative soft-tissue deformations using incomplete surface data and finite elements. IEEE Transactions on Medical Imaging 24(11), 1479–1491 (2005)
4. Samur, E., et al.: A robotic indenter for minimally invasive characterization of soft tissues. International Congress Series, vol. 1281, pp. 713–718 (2005)
5. Sanchez-Margallo, F.M., et al.: Anatomical changes due to pneumoperitoneum analyzed by mri: an experimental study in pigs. Surg. Radiol. Anat. 33(5), 389–396 (2011)
6. Bano, J., et al.: Simulation of pneumoperitoneum for laparoscopic surgery planning. In: Ayache, N., Delingette, H., Golland, P., Mori, K. (eds.) MICCAI 2012, Part I. LNCS, vol. 7510, pp. 91–98. Springer, Heidelberg (2012)
7. Bano, J., Hostettler, A., Nicolau, S.A., Doignon, C., Wu, H.S., Huang, M.H., Soler, L., Marescaux, J.: Simulation of the abdominal wall and its arteries after pneumoperitoneum for guidance of port positioning in laparoscopic surgery. In: Bebis, G., et al. (eds.) ISVC 2012, Part I. LNCS, vol. 7431, pp. 1–11. Springer, Heidelberg (2012)
8. Marescaux, J., et al.: Augmented-reality–assisted laparoscopic adrenalectomy. JAMA: The Journal of the American Medical Association 292(18), 2214 (2004)
9. Masamune, K., Sato, I., Liao, H., Dohi, T.: Non-metal slice image overlay display system used inside the open type MRI. In: Dohi, T., Sakuma, I., Liao, H. (eds.) MIAR 2008. LNCS, vol. 5128, pp. 385–392. Springer, Heidelberg (2008)
10. Clements, L.G., et al.: Organ surface deformation measurement and analysis in open hepatic surgery: method and preliminary results from 12 clinical cases. IEEE Transactions on Biomedical Engineering 58(8), 2280–2289 (2011)
11. Feuerstein, M., et al.: Intraoperative laparoscope augmentation for port placement and resection planning in minimally invasive liver resection. IEEE Transactions on Medical Imaging 27(3), 355–369 (2008)
12. Shekhar, R., et al.: Live augmented reality: A new visualization method for laparoscopic surgery using continuous volumetric computed tomography. Surgical Endoscopy, 1–10 (2010)
13. Nicolau, S.A., et al.: Augmented reality in laparoscopic surgical oncology. Surgical Oncology 20(3), 189–201 (2011)
14. Nozaki, T., et al.: Laparoscopic radical nephrectomy under near real-time three-dimensional surgical navigation with c-arm cone beam computed tomography. Surgical Innovation 19(3), 263–267 (2012)